Oceanic Response to Idealized Net Atmospheric Freshwater in the Pacific at the Decadal Time Scale*

BOYIN HUANG AND VIKRAM M. MEHTA

The Center for Research on the Changing Earth System, Columbia, Maryland

NIKLAS SCHNEIDER

International Pacific Research Center, and Department of Oceanography, University of Hawaii at Manoa, Honolulu, Hawaii

(Manuscript received 21 September 2004, in final form 23 May 2005)

ABSTRACT

In the study of decadal variations of the Pacific Ocean circulations and temperature, the role of anomalous net atmospheric freshwater [evaporation minus precipitation minus river runoff (EmP)] has received scant attention even though ocean salinity anomalies are long lived and can be expected to have more variance at low frequencies than at high frequencies. To explore the magnitude of salinity and temperature anomalies and their generation processes, the authors studied the response of the Pacific Ocean to idealized EmP anomalies in the Tropics and subtropics using an ocean general circulation model developed at the Massachusetts Institute of Technology. Simulations showed that salinity anomalies generated by the anomalous EmP were spread throughout the Pacific basin by mean flow advection. This redistribution of salinity anomalies caused adjustments of basin-scale ocean currents, which further resulted in basin-scale temperature anomalies due to changes in heat advection caused by anomalous currents. In this study, the response of the Pacific Ocean to magnitudes and locations of anomalous EmP was linear. When forced with a positive EmP anomaly in the subtropical North (South) Pacific, a cooling occurred in the western North (South) Pacific, which extended to the tropical and South (North) Pacific, and a warming occurred in the eastern North (South) Pacific. When forced with a negative EmP anomaly in the tropical Pacific, a warming occurred in the tropical Pacific and western North and South Pacific and a cooling occurred in the eastern North Pacific near 30°N and the South Pacific near 30°S. The temperature changes (0.2°C) in the tropical Pacific were associated with changes in the South Equatorial Current. The temperature changes (0.8°C) in the subtropical North and South Pacific were associated with changes in the subtropical gyres. The temperature anomalies propagated from the tropical Pacific to the subtropical North and South Pacific via equatorial divergent Ekman flows and poleward western boundary currents, and they propagated from the subtropical North and South Pacific to the western tropical Pacific via equatorward-propagating coastal Kelvin waves and to the eastern tropical Pacific via eastward-propagating equatorial Kelvin waves. The time scale of temperature response was typically much longer than that of salinity response because of slow adjustment times of ocean circulations. These results imply that the slow response of ocean temperature due to anomalous EmP in the Tropics and subtropics may play an important role in the Pacific decadal variability.

1. Introduction

Decadal-and-longer-time-scale climate variability in the Pacific Ocean, long-term variability of ENSO (see abbreviations in the appendix), and their physical mechanisms have attracted major attention from researchers in the last decade. Observations suggest that thermocline temperature anomalies propagated from the subtropical North Pacific to the tropical North Pacific during the 1960s and the 1990s (Deser et al. 1996; Schneider et al. 1999; Zhang et al. 1999; Hazeleger et al. 2001). While the observational evidence is not definitive, many mechanisms of the Pacific decadal variability and long-term variability of ENSO have been proposed. The major mechanisms are temperature anomalies advected from extratropics to the equator by ocean circulation in the thermocline (Gu and Philander 1997;

* Center for Research on the Changing Earth System Contribution Number 3 and International Pacific Research Center Contribution Number 337.

Corresponding author address: Dr. Boyin Huang, The Center for Research on the Changing Earth System (CRCES), 10211 Wincopin Circle, Suite 240, Columbia, MD 21044.
E-mail: byh@crces.org

Kleeman et al. 1999), coupling between the atmosphere and ocean (Latif and Barnett 1994, 1996; Jin 1997; Wu et al. 2003), stochastic atmospheric forcing (Frankignoul et al. 1997; Cessi and Louazel 2001; Junge et al. 2000), and nonlinear dynamics of the equatorial Pacific ocean–atmosphere system (Jin et al. 2003; Timmermann et al. 2003). Many of these studies focused on the interactions between ocean and atmosphere via wind stress and surface heat flux, but almost no attention has been paid to ocean–atmosphere interaction at the decadal time scale via net atmospheric freshwater [evaporation minus precipitation minus river runoff (EmP)].

The EmP affects the oceans via its impact on vertical mixing (Lindstrom et al. 1987; Lukas and Lindstrom 1991), density-compensated temperature and salinity anomalies (spiciness anomalies) in the thermocline (Schneider 2000, 2004; Yeager and Large 2004), and forcing the general circulation (Goldsbrough 1933; Stommel 1984; Huang 1993). Ocean responses to interannual EmP anomalies have been investigated by Huang and Mehta (2004, 2005). The possible role of EmP in El Niño events has been studied by Schneider and Barnett (1995) and Yang et al. (1999). The possible role of EmP and salinity in the coupling from the Tropics to the extratropics, however, has not been investigated. Salinity anomalies are long lived since they are not attenuated by ocean to atmosphere feedback (Hall and Manabe 1997) and, therefore, they can be transported to remote regions and influence ocean dynamics and thermodynamics in remote regions after a long time. Decadal ocean and climate variations can therefore occur because of transport of salinity anomalies created by EmP anomalies.

Estimates of precipitation and evaporation over the tropical and midlatitude oceans have been available since 1988 (Huffman et al. 1997; Chou et al. 1997). These estimates showed (Fig. 1a) that the average EmP anomalies between 1989 and 2000 (1989–2000 average minus 1988) were approximately 75 cm yr^{-1} in the tropical Pacific and the western subtropical Pacific. The negative EmP anomaly in the tropical Pacific would generally weaken the vertical mixing; and the temperature near the surface would, therefore, increase because of anomalous EmP forcing. The South Equatorial Current (SEC) would become weaker when the EmP anomaly was negative in the central and western equatorial Pacific; this would result in a reduction of cold advection from the western coast of Peru and, therefore, the surface temperature in the tropical Pacific would increase.

Sensitivity studies by Huang and Mehta (2004, 2005), however, showed that temperature (Fig. 1b) decreased 0.2°C in the tropical Pacific and changed 1°C in the subtropical Pacific in the Massachusetts Institute of Technology (MIT) OGCM. What caused the surface temperature in the tropical Pacific to decrease? The question motivated us to further quantify the Pacific Ocean's response to geographically localized EmP anomalies. We hypothesize that the surface temperature decrease in the tropical Pacific was driven remotely by the subtropical anomalous EmP, and further hypothesize that anomalous EmP may result in oceanic responses in salinity and temperature both locally (within a forcing region) and remotely (distant from a forcing region) at decadal time scale because of slow response times of ocean waves and advection.

To test our hypotheses, we designed a series of experiments with the MIT OGCM to quantify the Pacific Ocean's responses to changes in geographically localized EmP anomalies in the evaporation-excess subtropical regions in the North and South Pacific, and in the precipitation-excess equatorial region. The results of these experiments are described and discussed in this paper. The paper is organized as follows: A brief description of the MIT OGCM and experiment design is given in section 2. Local responses of salinity and temperature via vertical mixing in the forcing regions are described in section 3. Remote responses of salinity, temperature, and circulation via oceanic advection are described in section 4. The spiciness (salinity and temperature) anomalies along an isopycnal surface are investigated in section 5. Propagation of surface salinity and temperature anomalies, and changes in ocean circulation caused by these anomalies, are further explored in section 6. Sensitivity of the ocean responses to the strength of anomalous EmP and the imposed surface boundary condition is discussed in section 7. Results are summarized in section 8.

2. Model and experiments

The OGCM developed at MIT (Marshall et al. 1997; Huang et al. 2003; Huang and Mehta 2004, 2005) was used in the present study. The model domain is global with realistic topography. The latitudinal resolution is 0.4° near the equator, linearly increasing to 2° at and poleward of 20°S and 20°N. The longitudinal resolution is 2°. There are 30 levels in the vertical direction, with a resolution of 10 m between the ocean surface and 50-m depth, 25 m between 50 and 200 m, 50 m between 200 and 400 m, and 50–500 m below 400-m depth. The horizontal diffusivity is 10^3 m^2 s^{-1}. The vertical diffusivity and viscosity are calculated using the KPP method (Large et al. 1999).

The OGCM was "spun up" for 200 years from a motionless, initial state of annual-average temperature and salinity from Levitus and Boyer (1994) and Levitus et

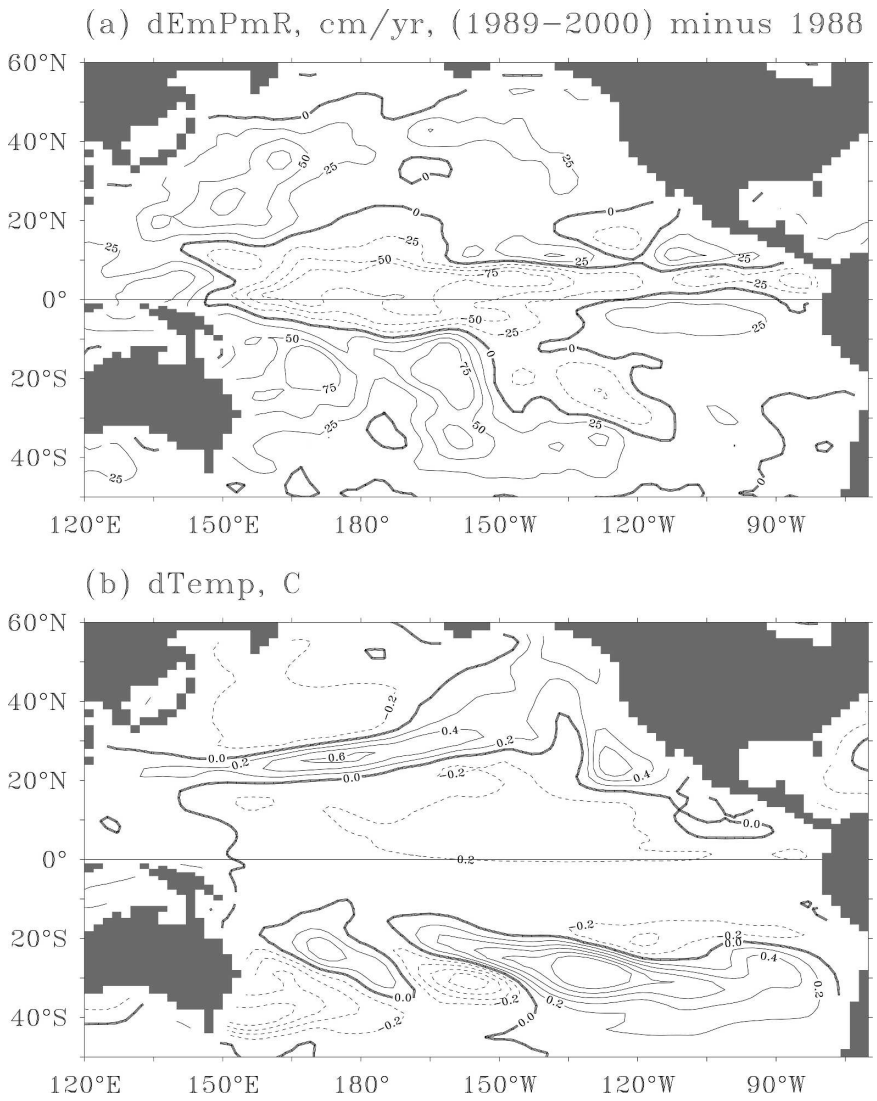

FIG. 1. Anomalies (1989–2000 average minus 1988 average) of (a) observed EmP anomaly and (b) simulated SST anomaly forced by anomalous EmP in (a). Contour intervals are 25 cm yr^{-1} in (a) and 0.2°C in (b). Negative values are dashed.

al. (1994). During the spinup, the OGCM was forced by monthly wind stress climatology from Hellerman and Rosenstein (1983). The first-layer salinity (S_1) was forced by monthly EmP climatology (Fig. 2), which consisted of satellite-based evaporation and precipitation between 50°S and 60°N from January 1988 to December 2000 (Huffman et al. 1997; Chou et al. 1997; Atlas et al. 1996; Huang and Mehta 2004) and runoff from 921 rivers into the global oceans (Dai and Trenberth 2002):

$$dS_1/dt = S_0(E - P - R)/\Delta z_1, \qquad (1)$$

where Δz_1 is the first-layer model thickness; S_1 was restored to monthly SSS of Levitus and Boyer (1994) poleward of 50°S and 60°N with a time scale of 60 days, because the satellite-based evaporation and precipitation are available only from 50°S to 60°N.

The first-layer temperature (T_1) was forced by a mixed boundary condition, which consists of a restoration to monthly SST and monthly net heat flux:

$$dT_1/dt = (\mathrm{SST} - T_1)/\tau_T + Q_{\mathrm{net}}/\rho c_p \Delta z_1, \qquad (2)$$

where SST is from Levitus and Boyer (1994); τ_T is a damping time scale of 10 days (equivalent to 50 W m^{-2} K^{-1} for the first layer thickness of 10 m); Q_{net} is from the Comprehensive Ocean–Atmosphere Dataset (da Silva et al. 1994). The mixed surface boundary condition [(2)] can simulate well both SST and net heat

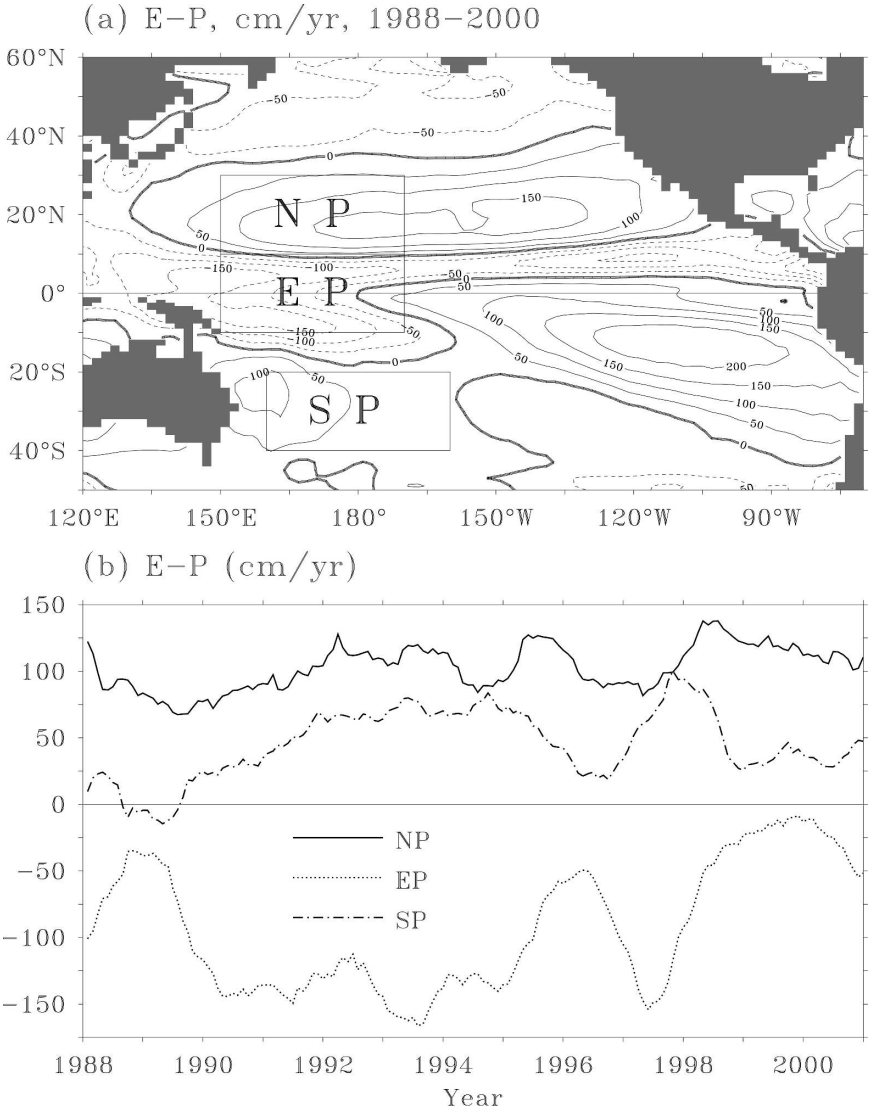

FIG. 2. (a) Climatological atmospheric freshwater. The contour interval is 50 cm yr^{-1}. Boxed NP, EP, and SP indicate forcing regions in the North Pacific, equatorial Pacific, and South Pacific. Their exact locations are listed in Table 1. (b) Evolution of EmP in regions NP, EP, and SP.

flux into the ocean. While the addition of freshwater to the ocean may imply the addition of heat, it is assumed here that the freshwater and the first layer of the ocean are at the same temperature. At the end of year 200, simulated annual-average salinity and temperature were reasonably close to the observed climatology in the Pacific Ocean near the surface; however, they were approximately 4°C and 1 psu higher than observations in the subtropical, subsurface Pacific Ocean. Substantially large errors in the subsurface Pacific Ocean were mainly due to strong vertical diffusion, which is a common problem in many GCMs (see, e.g., Jiang et al. 1999). The salinity error may also result from discrepancies between satellite-derived EmP estimate and the actual EmP climatology.

After the OGCM was spun up, the net heat flux into the ocean was diagnosed as

$$Q = \rho c_p \Delta z_1 (\mathrm{SST} - T_1)/\tau_T + Q_{\mathrm{net}}, \tag{3}$$

and the mixed surface boundary condition of (2) was changed into the flux boundary condition

$$dT_1/dt = Q/\rho c_p \Delta z_1 \tag{4}$$

in order to allow a SST perturbation to evolve according to ocean thermodynamics and dynamics. Using flux boundary conditions (1) and (4), the model was inte-

TABLE 1. Details of MIT OGCM experiments. Locations of EmP anomalies are shown in Fig. 2.

Expt	EmP anomaly			
	Magnitude (cm yr^{-1})	Duration (yr)	Location	Integration period (yr)
NP	100	5	150°E–170°W 10°–30°N	20
EP	−100	5	150°E–170°W 10°S–10°N	20
SP	100	5	160°E°–160°W 20°–40°S	20
ALL = NP + EP + SP		5		20
EP1	−100	1	As in EP	20
EP2	−540	2	As in EP	20
EP3	−100	3	As in EP	20
RST	As in ALL	5	As in ALL	20

grated further for 20 years, and this experiment is referred to as the CTR experiment.

To study effects of regional EmP anomalies (Fig. 1a) on salinity, temperature, and circulation of the upper Pacific Ocean, we designed four PTB experiments using idealized EmP anomalies in the NP (100 cm yr^{-1}), EP (−100 cm yr^{-1}), SP (100 cm yr^{-1}), and ALL (Table 1 and Fig. 2a) regions in addition to the climatological EmP. The idealized EmP anomalies were increased exponentially from zero to their final magnitude during the first 3 months, maintained at the final magnitude for 4½ yr, decreased exponentially to zero during the last 3 months, and maintained at zero thereafter to the end of the 20-yr experiments. The magnitude of anomalous EmP was based on time-averaged (Fig. 1a) and spatial-averaged (Fig. 2b) anomalous freshwater flux; the latter shows multiyear episodes of anomalous EmP at magnitudes of 80, 110, and 150 cm yr^{-1} in regions NP, SP, and EP (Fig. 1b), respectively. The location, however, was based on the climatological EmP shown in Fig. 2a. The difference between the PTB and CTR experiments is defined as the anomaly in this paper.

To test the sensitivity of oceanic responses to the magnitude and duration of anomalous EmP, further experiments were designed using different anomalous EmP forcing in the equatorial Pacific (EP1, EP3, and EP2 in Table 1). In EP1 and EP3, the minimum anomalous EmP was the same (−100 cm yr^{-1}) as in EP, but with shorter durations of 1 and 3 yr, respectively. In EP2, the minimum anomalous EmP was −540 cm yr^{-1} with a short duration of 2 yr, which resulted in −1080 cm anomalous EmP input to the ocean, twice as much as in EP (−500 cm). To test whether oceanic responses were sensitive to the surface heat flux boundary condition, another experiment was designed (RST, Table 1) in which the model SSTs were restored to observed monthly climatology from Levitus and Boyer (1994), using a restoring time of 60 days as shown in Eq. (3), which represents a heat flux damping of 8 W m^{-2} K^{-1} (Yang et al. 1999).

3. Local response to anomalous EmP

We first explore local responses of salinity and temperature, largely driven by vertical mixing, to anomalous EmP in experiments NP and EP. The local response in experiment SP is similar to that in experiment NP, and the response in experiment ALL is almost a linear combination of the three individual experiments.

When forced by a positive EmP anomaly in experiment NP, the local temperature and salinity respond in opposite signs before year 8 (Fig. 3a). Surface salinity increases and surface temperature decreases during the first 4 yr. After the anomalous forcing returns to zero, the ocean responds slowly and both salinity and temperature recover gradually. The effect of anomalous EmP forcing in the North Pacific eventually reaches the equatorial Pacific and the subtropical South Pacific, although their magnitudes of changes are relatively small. In addition to their long-term changes, salinity and temperature anomalies at seasonal time scale are also clear in Fig. 3 due to mean seasonal changes in vertical stratification and ocean currents.

When forced by a negative EmP anomaly in experiment EP, surface salinity decreases approximately 0.4 psu within the first 4 yr (Fig. 3b). As anomalous EmP forcing returns to zero, surface salinity recovers quickly between year 4 and 8. Temperature, however, responds differently. The temperature anomaly between 0 and 50 m increases to about 0.2°C during the first 8 yr. It then decreases slowly over the next decade. This behavior suggests that there is a slow temperature response, relative to salinity response, of the tropical Pacific to anomalous EmP. The salinity and temperature anoma-

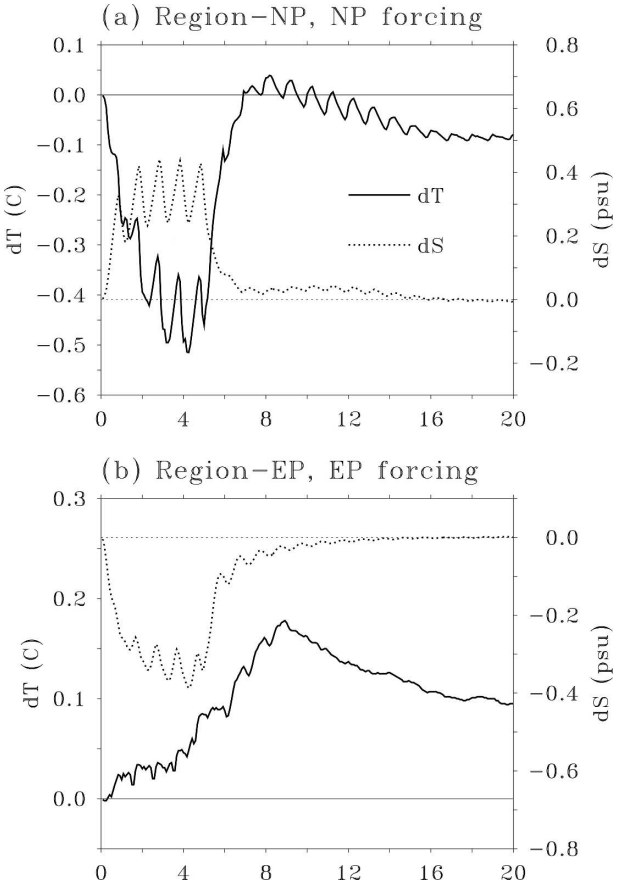

FIG. 3. Surface (0–50 m) temperature (left coordinate, °C) and salinity (right coordinate, psu) anomalies at (a) region NP in expt NP and (b) region EP in expt EP.

lies eventually reach the subtropical North and South Pacific. This is described further in the next section. From Figs. 3a and 3b, it is clear that the correlation between temperature and salinity anomalies is largely negative within the local forcing regions before year 8, which is consistent with the studies by Yang et al. (1999) and Huang and Mehta (2004).

To understand the physical mechanisms controlling the salinity and temperature changes, the total (local) changes of salinity and temperature were integrated based on terms of advection and vertical mixing:

$$(\Delta S, \Delta T)_{\text{total}} = \sum_0^t \partial_t(S, T)\delta t, \tag{5}$$

$$(\Delta S, \Delta T)_{\text{adv}} = \sum_0^t [-u\partial_x(S, T) - v\partial_y(S, T) - w\partial_z(S, T)]\delta t, \quad \text{and} \tag{6}$$

$$(\Delta S, \Delta T)_{\text{mix}} = \sum_0^t (S_{\text{mix}}, T_{\text{mix}})\delta t, \tag{7}$$

where the terms on the right-hand side of (5)–(7) are anomalies between the PTB and CTR experiments; $\partial_t(S, T)$ are total (local) changes of salinity and temperature and δt is the time interval of 1 month between model diagnosis outputs averaged every month from the terms calculated at each time step;

$$S_{\text{Mix}} = \partial_{zz}S + S_{\text{KPP}} + S_0(E - P - R)/\Delta z_1 \quad \text{and} \tag{8}$$

$$T_{\text{Mix}} = \partial_{zz}T + T_{\text{KPP}} + Q/(\rho c_p \Delta z_1), \tag{9}$$

represent the vertical mixing of salinity and temperature. Here, $\partial_{zz}(S, T)$ are vertical diffusion and $(S, T)_{\text{KPP}}$ are nonlocal diffusion due to KPP mixing. The combination of terms in advection and vertical mixing is based on their similarity of dynamic properties and the fact that advection is largely compensated in three dimensions, as well as the vertical and KPP mixing. The source terms of EmP and surface heat flux are included in vertical diffusion as upper surface boundary conditions. By comparing the sign and tendency of anomalies due to advection and vertical mixing with those of total anomalies, it is easy to see the relative importance of advection and vertical mixing contributing to the total variabilities at the decadal time scale.

Analyses of the various terms mentioned above indicate that the described salinity changes are due to vertical mixing in regions NP and EP (Fig. 4) of anomalous EmP forcing in experiments NP and EP, respectively. The magnitude of salinity change due to anomalous vertical mixing dominates over that due to anomalous advection, although anomalous advection itself is strong because of the integrating effect as shown in (6). The salinity anomalies in regions NP and SP, driven by local vertical mixing, eventually reach other remote regions via mean ocean circulation.

Local temperature change (Fig. 5) is driven by vertical mixing in region NP and by heat advection in region EP in experiments NP and EP, respectively. Further decomposition of total advection (Fig. 6a) shows that the local warming in experiment EP is largely associated with meridional heat advection due to anomalous convergent flow. The vertical heat advection also contributes to the warming because of the increase of downwelling after anomalous EmP relaxes after year 4. In remote regions, temperature anomalies are driven largely by heat advection due to anomalous ocean circulation, which, in turn, is associated with a redistribution of salinity anomalies caused by mean ocean circulation. For example, forced by anomalous EmP in the subtropical Pacific in experiment NP, temperature decreases in region EP, which is driven by zonal and meridional heat advection (Fig. 6b).

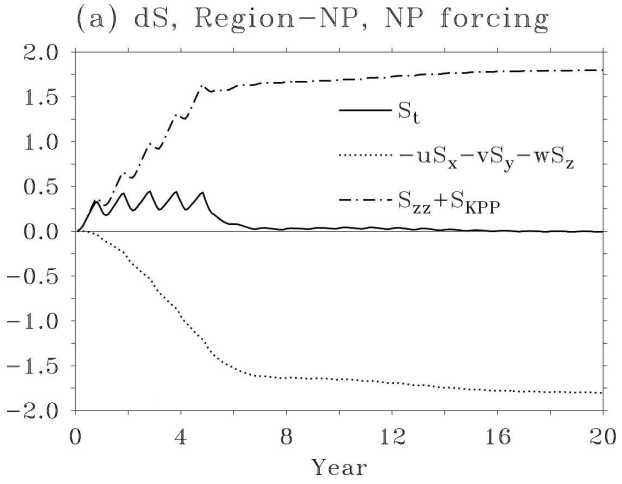

FIG. 4. Terms of surface (0–50 m) salinity equation (psu) at (a) region NP in expt NP and (b) region EP in expt EP.

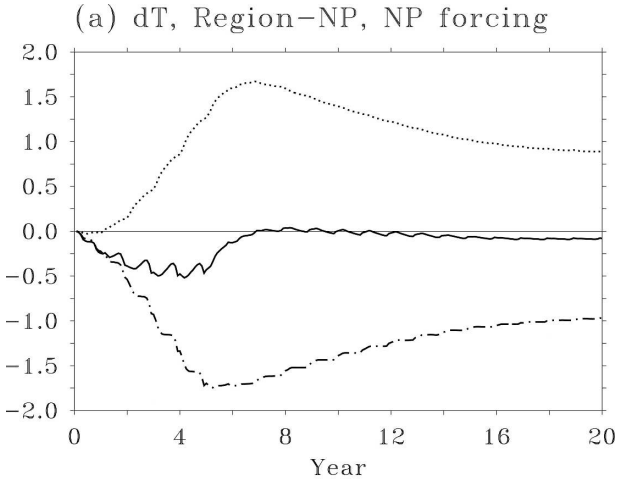

FIG. 5. As in Fig. 4, but for terms of surface (0–50 m) temperature equation (°C).

Briefly, EmP locally affects salinity directly and temperature through changes of vertical mixing. These anomalous tendencies are balanced by changes of advection and waves that move the anomalies to remote regions.

4. Nonlocal response to anomalous EmP

To assess the overall nonlocal oceanic response to anomalous EmP forcing, we first present the average (20 yr, 0–50 m) anomalies of SSS and SST in experiments NP, EP, SP, and ALL. As indicated in Fig. 3, salinity and temperature anomalies become relatively steady after year 8, their final states (average between year 9 and 20) are very similar to 20-yr averages (not shown).

Forced by a positive EmP anomaly in experiment NP, much of the saltier water drifts along the mean ocean circulation from the western Pacific toward the east in the subtropical gyre (Fig. 7a). Therefore, SSS increases approximately 0.2 psu in the North Pacific between 15° and 35°N.

Corresponding to this SSS change in experiment NP, the subtropical gyre circulation becomes weaker, and the SEC becomes stronger (Fig. 8a). The weakening of the subtropical gyre circulation due to anomalous EmP is consistent with the Stommel–Goldsbrough circulation (Goldsbrough 1933; Stommel 1984; Huang 1993). The major reason for weakening subtropical gyres in the Pacific is the higher density or heavier water within the gyre due to a positive EmP anomaly since the monthly climatology of the wind forcing was specified. Another reason is the stronger vertical mixing resulting from saltier surface water due to positive EmP anomaly, which can more effectively transport momentum fluxes from the surface to the deeper layer; therefore, the subtropical gyre near the surface is weakened. The stronger SEC is largely associated with a stronger

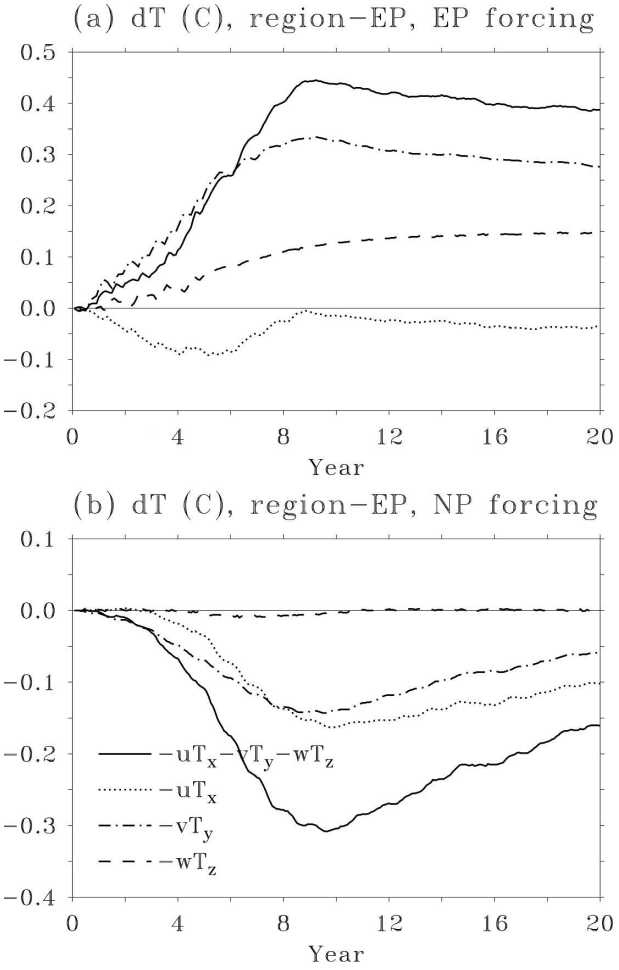

FIG. 6. Advection terms of surface (0–50 m) temperature (°C) equation in region EP in (a) expt EP and (b) expt NP.

zonal density gradient due to the redistribution of salinity, which is consistent with Huang (1993).

The anomalous ocean currents in experiment NP further result in changes in temperature. It is clear that the weakening of the Kuroshio is associated with a cooling (0.3°–0.5°C) in the western North Pacific (Fig. 8a); the weaker equatorward interior flows in the eastern North Pacific cause a warming (0.4°C) due to reduced cold advection. The cooling (0.1°C) in the tropical Pacific is caused by increased cold advection due to a stronger SEC.

Forced by a negative EmP anomaly in experiment EP, average SSS (Fig. 7b) decreases 0.1 psu in the western North and South Pacific. Even though the anomalous EmP is located near the equator, SSS anomalies develop in the tropical Pacific, as well as in the subtropical North and South Pacific. The reason is that salinity anomalies drift poleward from the EP region due to mean divergent Ekman flows near the equator. Corresponding to the SSS changes in experiment EP, the subtropical gyre circulation becomes stronger and the SEC becomes weaker (Fig. 8b), which appears to be opposite to those in experiment NP according to the Stommel–Goldsbrough theory due to reversed EmP forcing. The poleward transport of fresher water from the tropical Pacific results in lighter surface water or weaker vertical mixing, which results in a stronger gyre circulation. Since the surface water in the western Pacific becomes fresher and therefore lighter, the SEC becomes stronger. It is the anomalous gyre circulation and SEC that result in anomalous ocean temperatures. The warmings in the western North (0.3°C) and South (0.1°C) Pacific result from increased warm advection due to a stronger Kuroshio and a stronger EAC. The coolings (0.1°–0.2°C) in the eastern North and South Pacific result from increased cold advection due to stronger equatorward branches of the subtropical gyres. In the equatorial Pacific, the warming (0.1°C) is largely associated with reduced cold advection due to a weaker SEC. The warming in the western equatorial Pacific appears to be associated with an anomalous meridional convergent flow (Fig. 8b) as well as a weaker SEC.

The surface salinity and temperature anomalies can penetrate below 500 m. For example, between 250 and 500 m, temperature anomalies (Fig. 9a) are at magnitude of 0.2°C in the North Pacific in experiment NP. The temperature anomalies in the eastern subtropical North Pacific near the surface (Figs. 8a and 8b) have moved toward the western tropical Pacific between 250 and 500 m (Figs. 9a and 9b). Therefore, the east–west oriented temperature anomalies in the subtropical Pacific near the ocean surface become north–south oriented in the subsurface ocean.

The spatial structures of temperature anomalies (Figs. 7c, 8c, and 9c) due to a positive EmP anomaly in experiment SP are very similar to those in experiment NP. The major difference is that temperature anomalies are slightly larger and penetrate deeper when they are forced by anomalous EmP in the South Pacific. The reason is that the thermocline slope in the forcing region in experiment SP is steeper than that in experiment NP. The temperature anomalies (Figs. 8d and 9d) due to combined forcing in experiment ALL are almost a linear superposition of those due to each individual forcing. The experiments NP, SP, and EP have verified our hypothesis that the cooling in the tropical Pacific in Fig. 1b is indeed caused remotely by a positive EmP anomaly in the subtropical North and South Pacific. The spatial structures of anomalous salinity and temperature due to the combined forcing also exhibit some similarities to those forced by the observed EmP

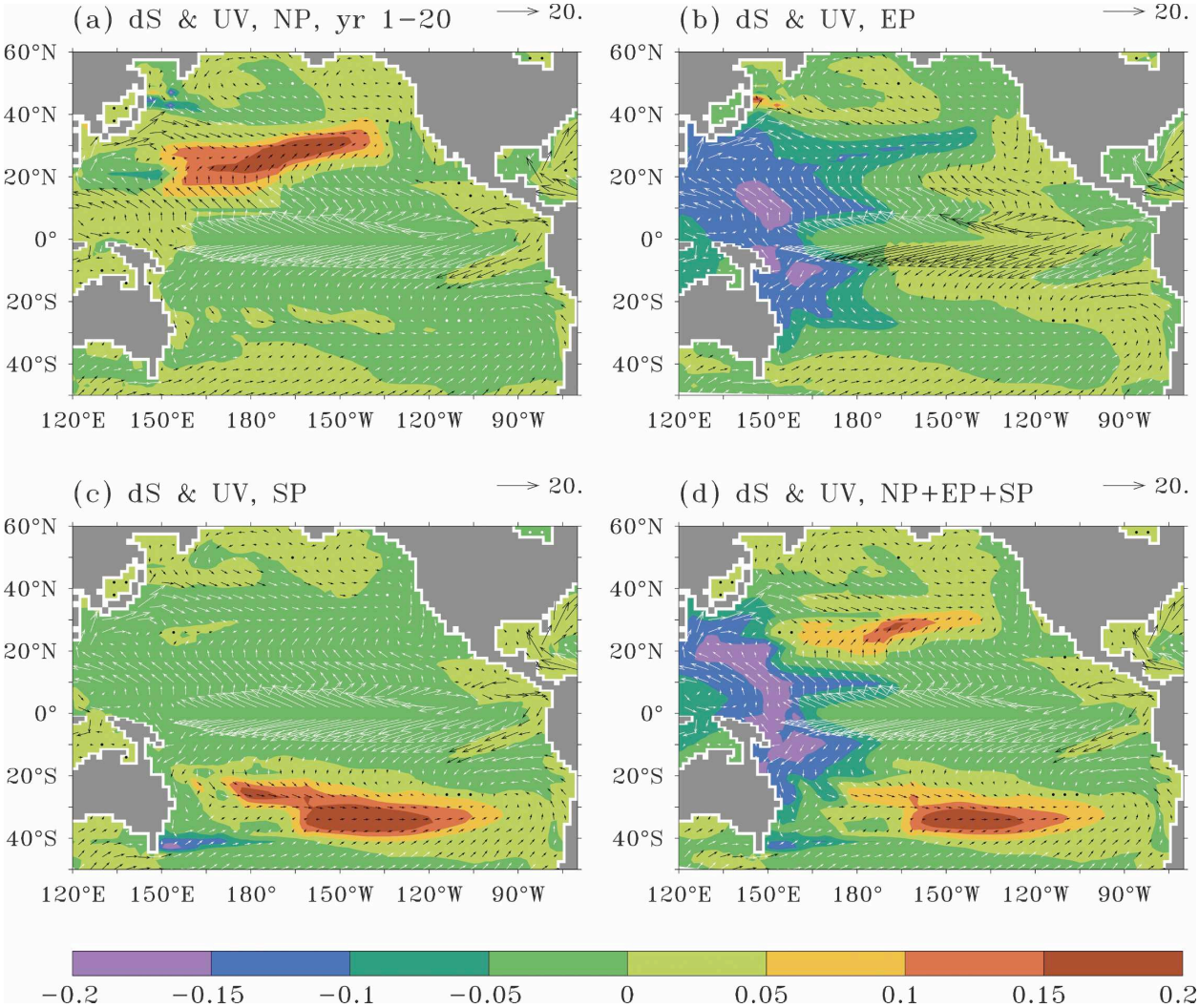

FIG. 7. Average (1–20 yr) surface (0–50 m) salinity anomaly and mean ocean currents in (a) expt NP, (b) expt EP, (c) expt SP, and (d) expt ALL. The contour interval is 0.05 psu. Vector scales are indicated at upper right (cm s^{-1}). Vector colors are for visual purpose only.

anomalies (e.g., Fig. 1a) in Huang and Mehta (2005). The reason is that the spatial structures of idealized EmP anomalies are constructed to be similar to the observed EmP anomalies.

5. Spiciness

The density anomalies due to the salinity and temperature anomalies in our experiments indicate that changes in density due to anomalous salinity are largely compensated by those due to anomalous temperature below 800 m or the 27.3-σ_θ isopycnal surface. The density anomalies above 800 m, however, are substantially changed by anomalous EmP. The spiciness (salinity and temperature) anomalies penetrate from the subtropical Pacific to the tropical Pacific along the isopycnal surface in the thermocline as proposed by Schneider (2000), for example, along the 26-σ_θ isopycnal.

Forced by a positive EmP anomaly in experiment NP, an elongated salinity anomaly (0.2 psu) on the 26-σ_θ isopycnal develops, during the 20-yr experiment, a northeast–southwest direction in the North Pacific (Fig. 10a). This indicates that the high-salinity subtropical water penetrates to the tropical Pacific in the thermocline along the 26-σ_θ isopycnal via the western boundary exchange window (Liu 1994; Lu and McCreary 1995; Huang and Liu 1999). A temperature anomaly (0.5°C, not shown) is found at the same isopycnal to compensate for the salinity anomaly.

Forced by a negative EmP anomaly in experiment EP, salinity anomalies (−0.1 psu) penetrate from the subtropical North and South Pacific toward the western

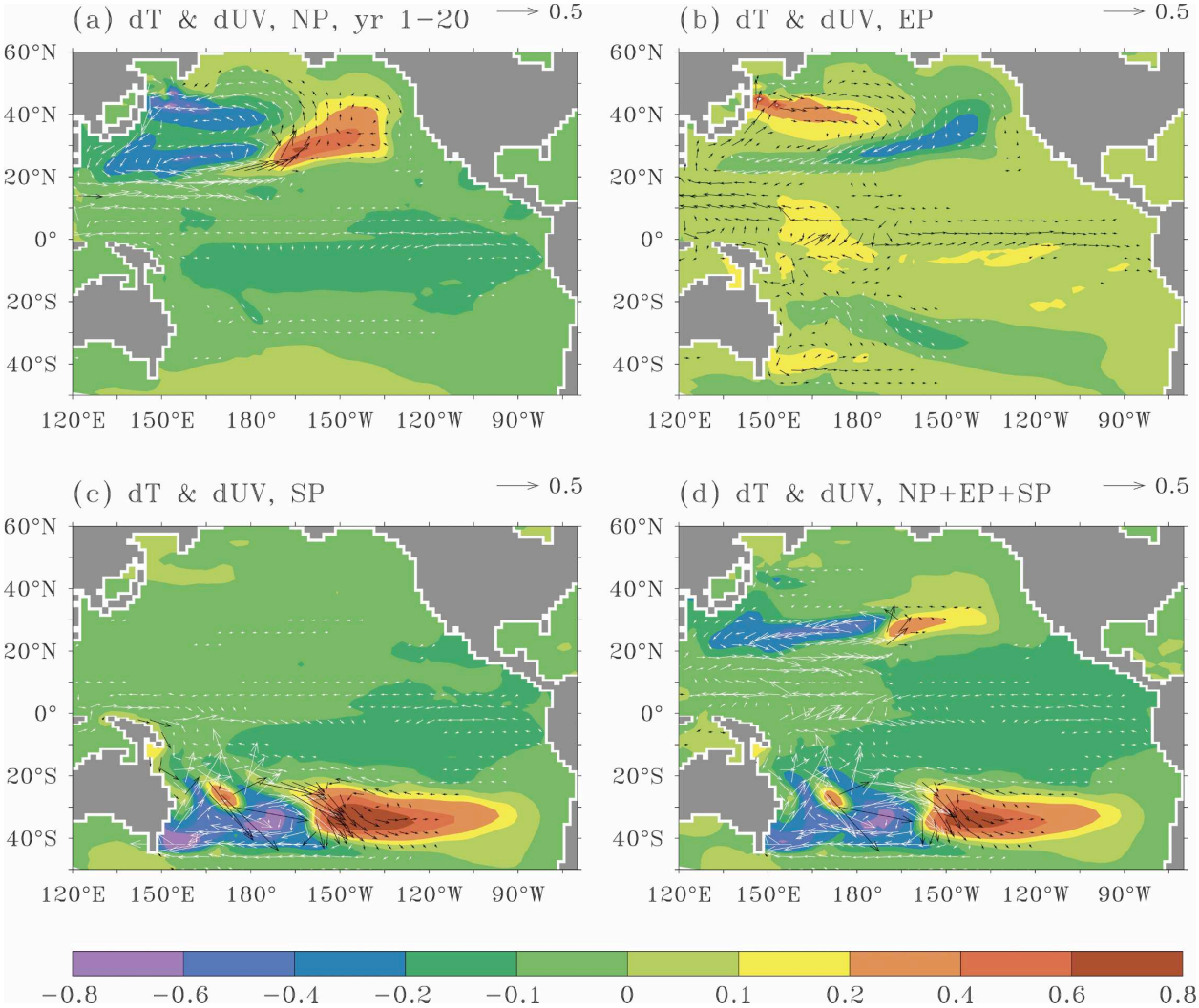

FIG. 8. Average (1–20 yr) surface (0–50 m) temperature anomaly (shaded; °C) and anomalous ocean currents (vectors) in (a) expt NP, (b) expt EP, (c) expt SP, and (d) expt ALL. Vector scales are indicated at upper right (cm s^{-1}). Vector colors are for visual purpose only.

tropical Pacific on the 26-σ_θ isopycnal (Fig. 10b). As indicated in Fig. 7b, the negative salinity anomalies originate from the tropical Pacific near the surface and are transported to the subtropical North and South Pacific via the mean ocean circulation. A temperature anomaly (–0.1°C to −0.2°C) is found on the same isopycnal surface (not shown).

Forced by a positive EmP anomaly in experiment SP, the salinity anomalies (Fig. 10c) are similar to those in experiment NP. The salinity anomalies in experiment ALL (Fig. 10d) are, again, almost a linear superposition of those in the three individual experiments.

Associated with the anomalous EmP forcing, water density changes in both local and remote regions, indicating a change in the depth of isopycnal surface as shown in Fig. 11 for the 26-σ_θ isopycnal. The 26-σ_θ isopycnal shoals (deepens) about 50 m in the northwestern North Pacific in experiment NP (EP). It should be noted that the largest change in the depth of the 26-σ_θ isopycnal surface is located in the subtropical Pacific, even when an EmP forcing is applied in the tropical Pacific as indicated in experiment EP (Fig. 11b). The reason is that the saltier water in the tropical Pacific due to anomalous EmP is largely transported to the subtropical Pacific by mean ocean currents; and the saltier water shoals the isopycnal.

6. Propagation of salinity and temperature anomalies

Salinity anomalies between the surface and 50 m due to a positive EmP anomaly in experiments NP and SP

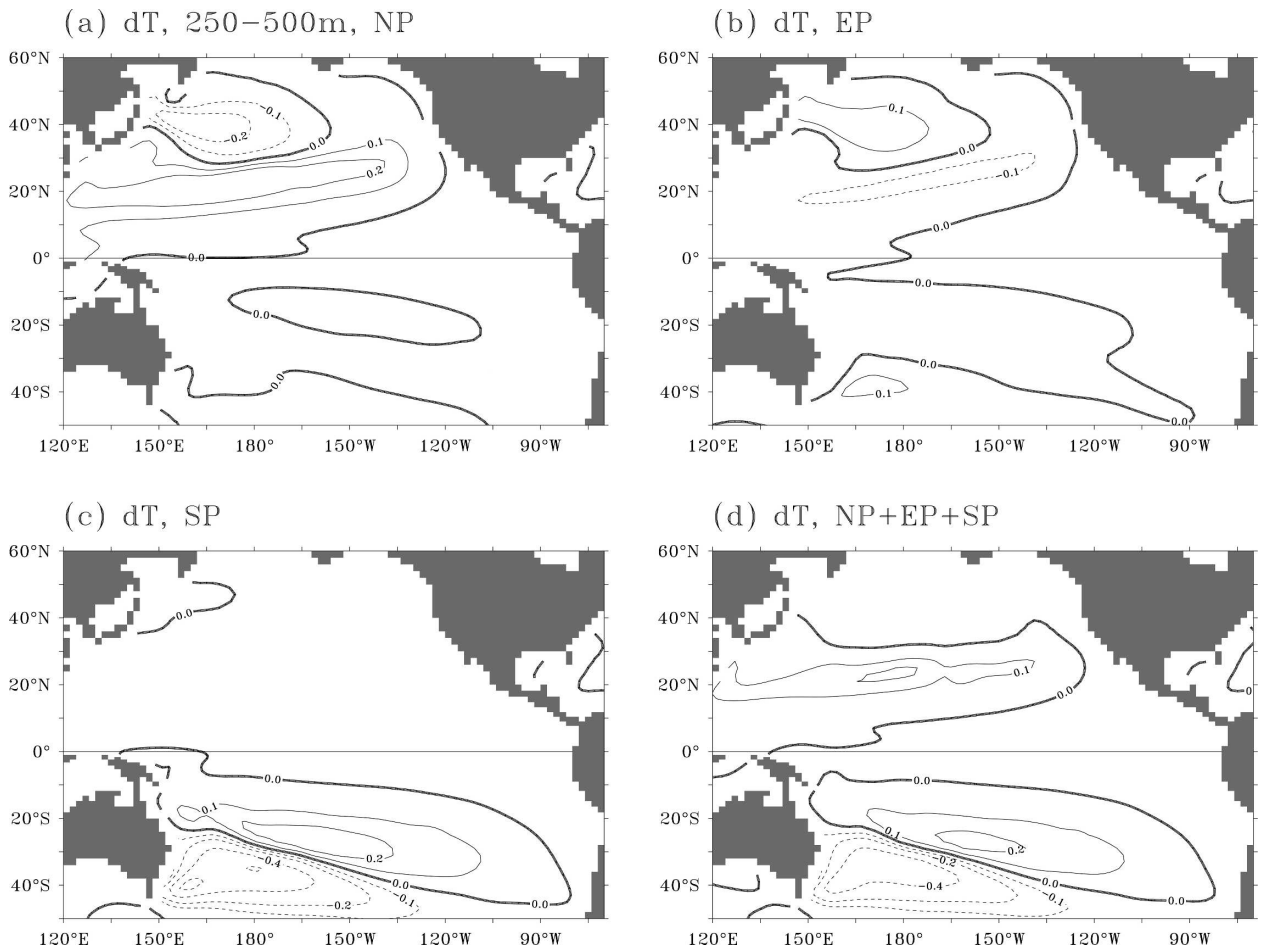

FIG. 9. Average (1–20 yr) temperature anomaly between 250 and 500 m in (a) expt NP, (b) expt EP, (c) expt SP, and (d) expt ALL. Contours are ±0.1, ±0.2, ±0.4, and ±0.6°C.

appear to be trapped within the subtropics (Figs. 12a and 12c). Forced by a negative EmP anomaly in experiment EP, surface salinity anomalies propagate toward the subtropical North and South Pacific at a speed of approximately 2 cm s^{-1} (Figs. 12b and 12d). In contrast to salinity anomalies, surface temperature anomalies propagate both poleward and equatorward (Fig. 13).

Forced by a positive EmP anomaly in experiments NP and SP (Figs. 13a and 13c), a cold temperature anomaly between surface and 50 m is generated due to stronger vertical mixing in the subtropical latitudes. This cold anomaly is largely confined within the subtropical North (20°–30°N) and South (20°–40°S) Pacific as salinity anomalies shown in Figs. 12a and 12c. A warm anomaly emerges in the subtropical Pacific after year 5, associated with the spindown of the equatorward subtropical gyre circulations as indicated in Figs. 8a and 8c. The weakening of the Kuroshio and EAC also contributes to the subtropical cooling in the western North and South Pacific. In addition, a cold temperature anomaly (approximately 0.1°C) appears in the tropical Pacific after year 4, which appears to be separate from the subtropical cooling and is further analyzed later in this section.

Forced by a negative EmP in experiment EP (Fig. 13b), a warm anomaly is generated in the tropical Pacific near the surface due to reduced cold advection by a weaker SEC after year 3. It propagates poleward and reaches 20°N in the North Pacific and 20°S in the South Pacific by year 10 due to the divergent Ekman flows in the equatorial Pacific, and Kuroshio and EAC along the western boundaries. In addition, cold temperature anomalies are generated in the subtropical North and South Pacific, in experiments NP and SP respectively, after year 6 due to changes in the respective subtropical gyre circulation. Forced by the combined equatorial and tropical–subtropical EmP anomalies in experiment ALL, Fig. 13d synthesizes the propagation of temperature anomalies between tropical and subtropical Pa-

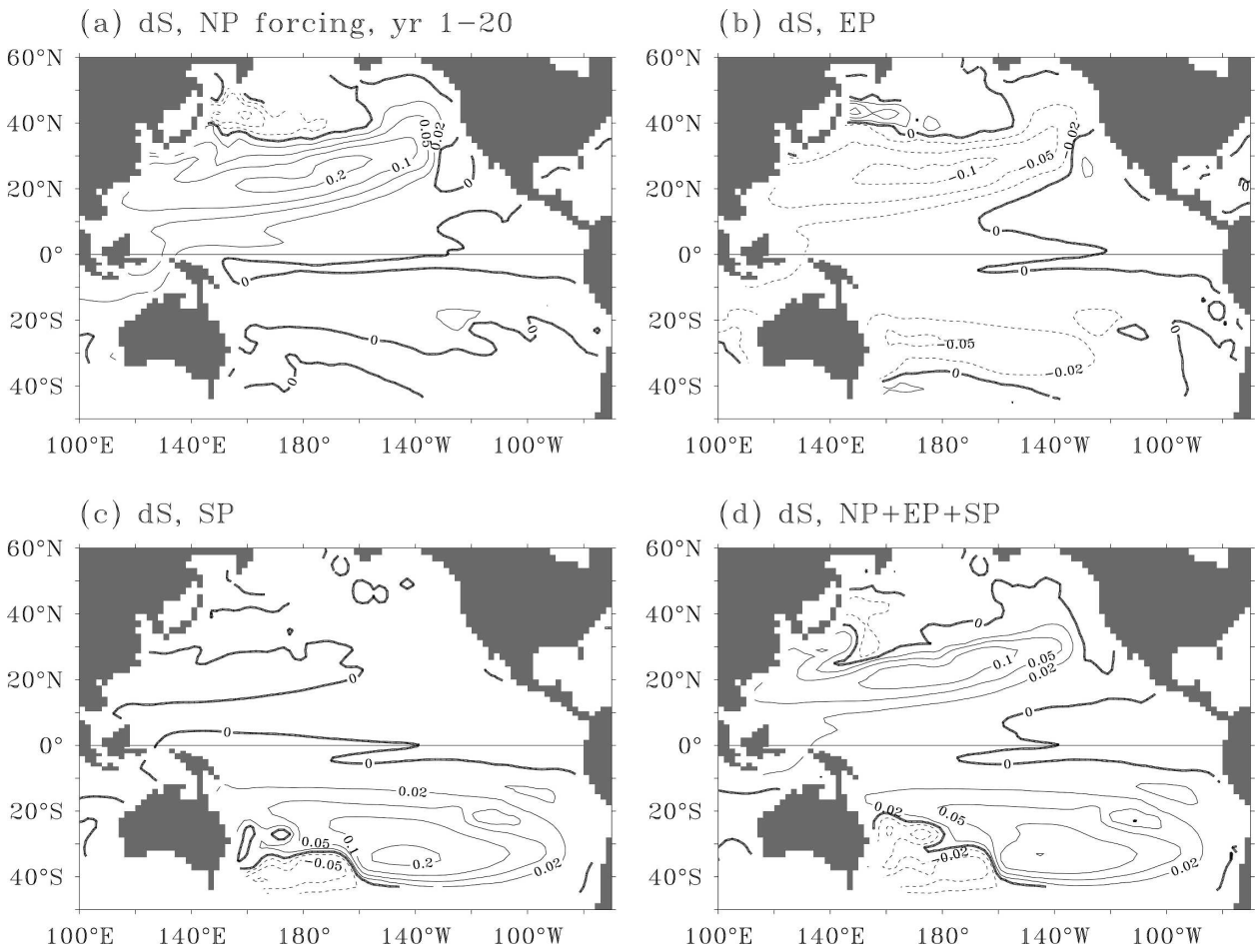

FIG. 10. Average (1–20 yr) salinity anomaly on the 26-σ_θ isopycnal in (a) expt NP, (b) expt EP, (c) expt SP, and (d) expt ALL. Contours are 0, ±0.02, ±0.05, ±0.1, and ±0.2 psu. The anomaly is calculated from time-dependent monthly output.

cific, which again is approximately a linear combination of three individual EmP forcings in the tropical and subtropical Pacific.

The mechanisms controlling the propagation of the temperature anomalies are shown in a sequence of their evolutions along the 26-σ_θ isopycnal over a 3-yr period. Forced by a positive EmP anomaly in experiment NP, a cold temperature anomaly is generated near the surface due to stronger vertical mixing in the western North Pacific and it reaches the western boundary at year 3 (Fig. 14a). The weak cold temperature anomaly then travels southward along the western boundary and eastward along the equator (Figs. 14a and 14b). This cold temperature anomaly strengthens and travels westward (Fig. 14c). It appears that this cold temperature anomaly is generated primarily by coastal Kelvin waves propagating southward along the western boundary and Kelvin waves propagating eastward along the equator. After the Kelvin waves reach the eastern boundary, Rossby waves are excited and propagate toward the western tropical Pacific while stretching toward higher latitudes. This might be the reason why the cold anomaly in the eastern tropical Pacific is stronger than that in the west. In the meantime, a warm temperature anomaly is found east of the cold anomaly in the subtropical North Pacific, which is primarily due to the spindown of the subtropical gyre circulation in the interior ocean (see Fig. 8a). The warm anomaly stretches southwestward toward the western tropical Pacific (Figs. 14a–c) in the subtropical gyre.

Forced by a negative EmP anomaly in experiment EP, a weak cold anomaly develops near the surface due to weaker vertical mixing in the western equatorial Pacific at year 1 (Fig. 14d). The cold anomaly stretches poleward, as does the salinity anomaly above the 26-σ_θ isopycnal. In addition, a separate warm anomaly appears in the eastern tropical Pacific after year 2, which apparently results from Kelvin waves propagating eastward along the equator as in experiment NP. After Kelvin waves reach the eastern boundary, Rossby

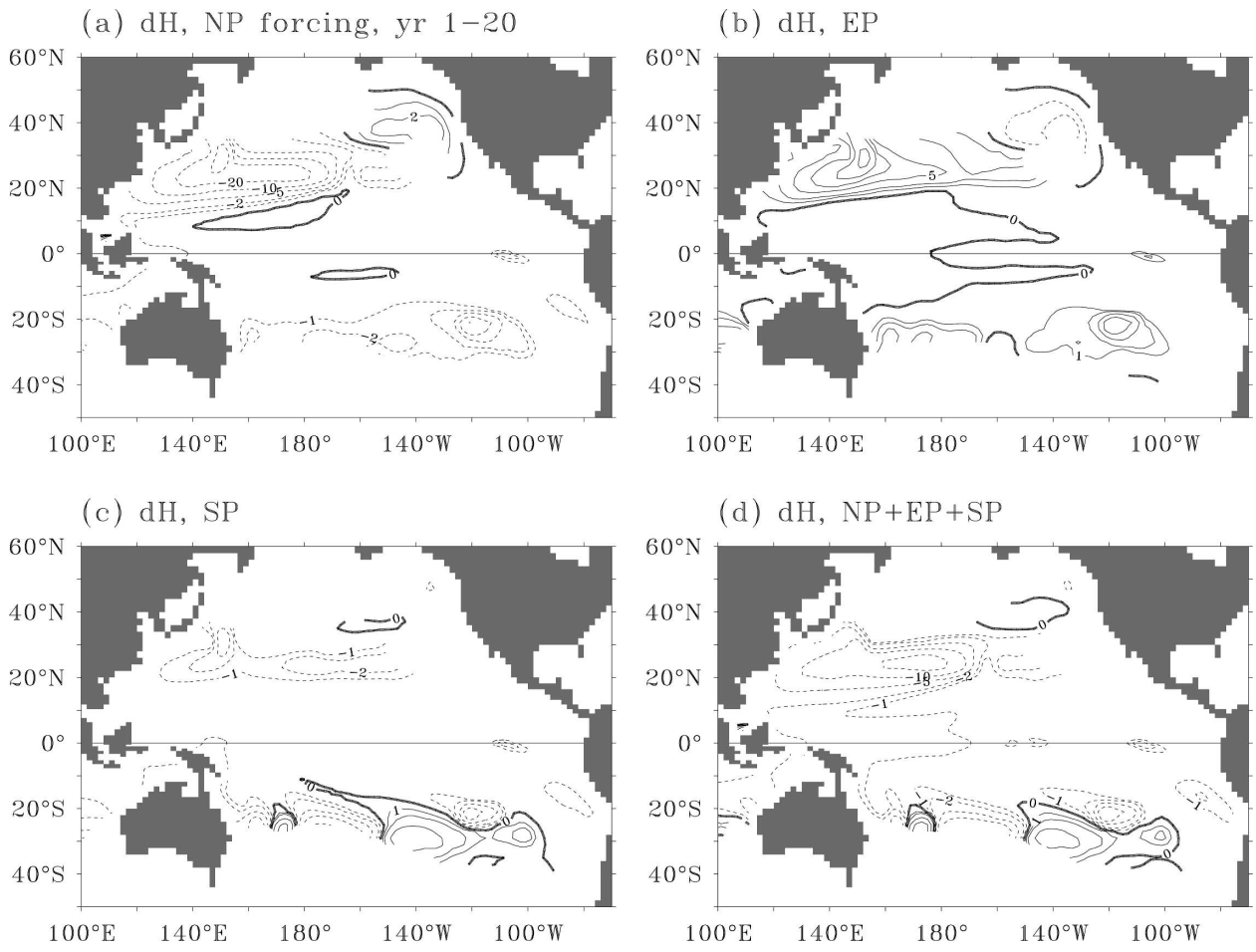

FIG. 11. As in Fig. 10, but for depth anomaly of the 26-σ_θ isopycnal. Contours are 0, ±1, ±2, ±5, ±10, ±20, and ±50 m. Negative values represent shoaling.

waves are excited and the SEC weakens because of an increase in the east–west density gradient, which results from the negative EmP anomaly in the western equatorial Pacific. Therefore, a warm anomaly (Figs. 14e and 14f) develops in the eastern equatorial Pacific due to reduced cold advection and travels westward by the SEC and equatorial Rossby waves. Eventually, the warm and cold anomalies become relatively stable for longer than a decade because of slower response in ocean currents. The response to a positive EmP anomaly in experiment SP is very similar (not shown) to that in the North Pacific. The effect of the combined forcing in experiment ALL (not shown) is nearly a linear combination of responses due to the three individual forcings.

7. Discussion

The evolution of the temperature anomalies described in the previous section raises a question: why do the temperature anomalies originating in the western North and South Pacific reach the equatorial Pacific but the salinity anomalies are confined to the North and South Pacific? The reason is that the subtropical gyres spin down when they are forced by a positive EmP anomaly. As a result, the temperature anomalies (cooling in the west and warming in the east) develop easily due to strong anomalous heat advection (Figs. 8a and 8c) since the meridional gradient of mean temperature is large. As the cooling in the western North or South Pacific reaches the western boundary, it can propagate toward the equator via coastal Kelvin waves. In contrast, the spindown of the subtropical gyres does not generate strong salt advection since the mean salinity distribution does not have a large gradient along the subtropical gyre circulations in the western Pacific. Therefore, positive salinity anomalies shown in Figs. 7a and 7c are forced purely by anomalous local EmP, and salinity anomalies do not develop because of weak anomalous salt advection. As a result, salinity anomalies do not reach the western boundary. Another factor

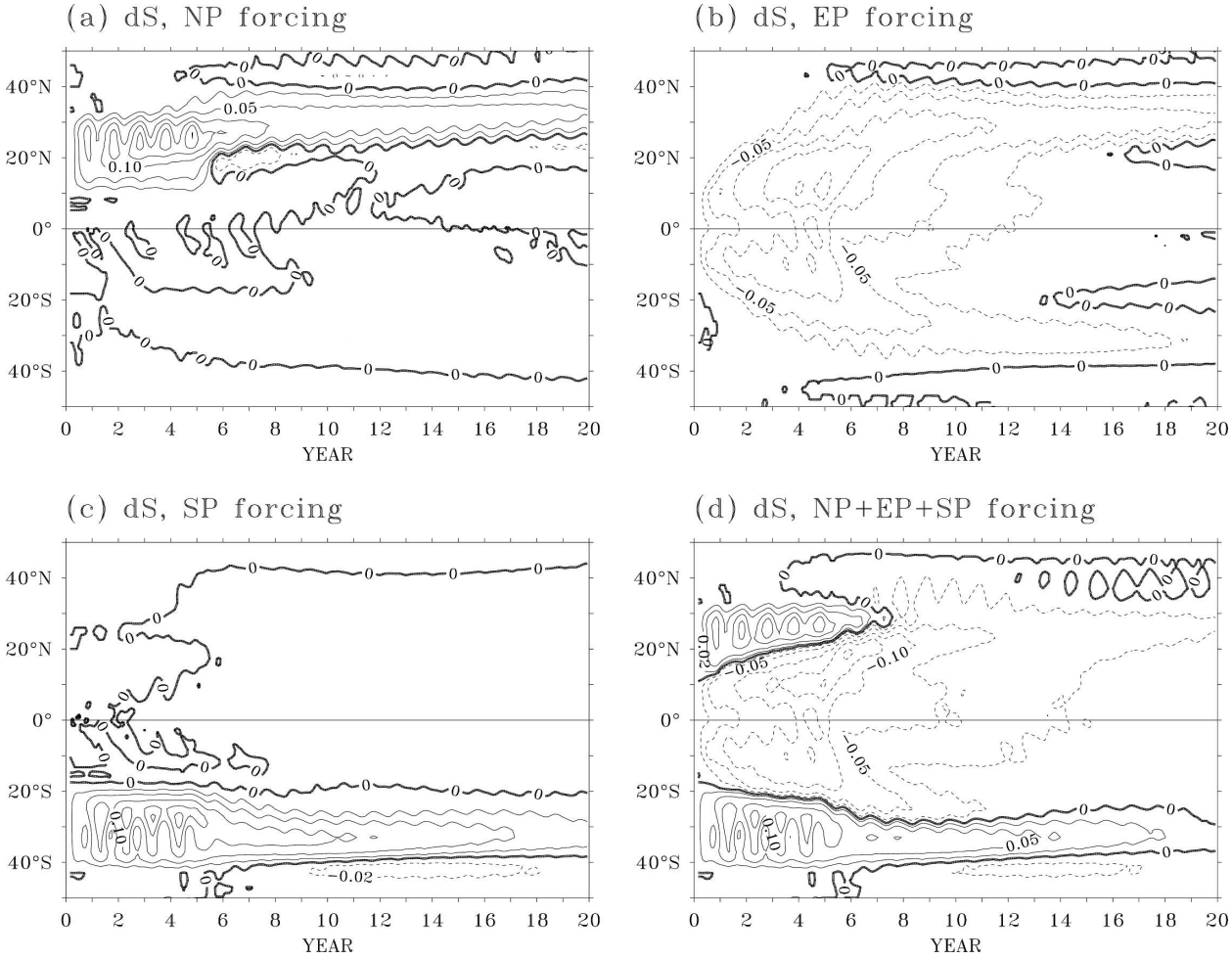

FIG. 12. Zonal mean salinity anomaly above 50 m in (a) expt NP, (b) expt EP, (c) expt SP, and (d) expt ALL. Contours are 0, ±0.02, ±0.05, ±0.1, ±0.15, and ±0.2 psu.

prohibiting the development of salinity anomalies is the compensation of anomalous salinity advection in three dimensions. For example, in the eastern equatorial Pacific, the changes in the SEC are very clear when forced by anomalous EmP in the equatorial, North, or South Pacific (Fig. 8), which results in temperature anomalies in the eastern equatorial Pacific. More detailed analyses indicate, however, that the salinity anomalies due to zonal salt advection are largely compensated by either meridional or vertical salt advection. Therefore, the effect of anomalous currents on salinity is very different from that on temperature because of differences of spatial structures of climatological salinity and temperature.

Since the strength of the anomalous EmP forcing in our experiments is stronger than in reality, we further tested the sensitivity of oceanic responses to the integrated strengths (magnitude and duration) of anomalous EmP. We conducted three more experiments (EP1, EP2, and EP3; Table 1) with different EmP strengths in region EP. Although the spatial structures of the oceanic response in EP1, EP2, and EP3 are similar to those in experiment EP, the amplitude and time scale of responses are different. For example, salinity anomalies in region EP (Fig. 15a) become weaker and last for a shorter time when the duration of anomalous EmP is shorter in EP3 (3 yr) and EP1 (1 yr). Temperature anomalies (approximately 0.02°, 0.06°, 0.1°, and 0.23°C) in EP1, EP3, EP, and EP2 at year 20 (Fig. 15b) appear to be linearly proportional to the magnitude of total anomalous EmP (−100, −300, −500, and −1080 cm). The linearity of the oceanic responses to different integrated strengths of anomalous EmP can also be seen when the response to the combined EmP forcing is compared with the responses to individual EmP forcing as shown in Fig. 8. The experiments EP1, EP3, EP, and EP2 also indicated that when the duration of anomalous EmP is shorter (e.g., 2 yr in EP2), the oceanic responses can be distinguished into a fast response (first

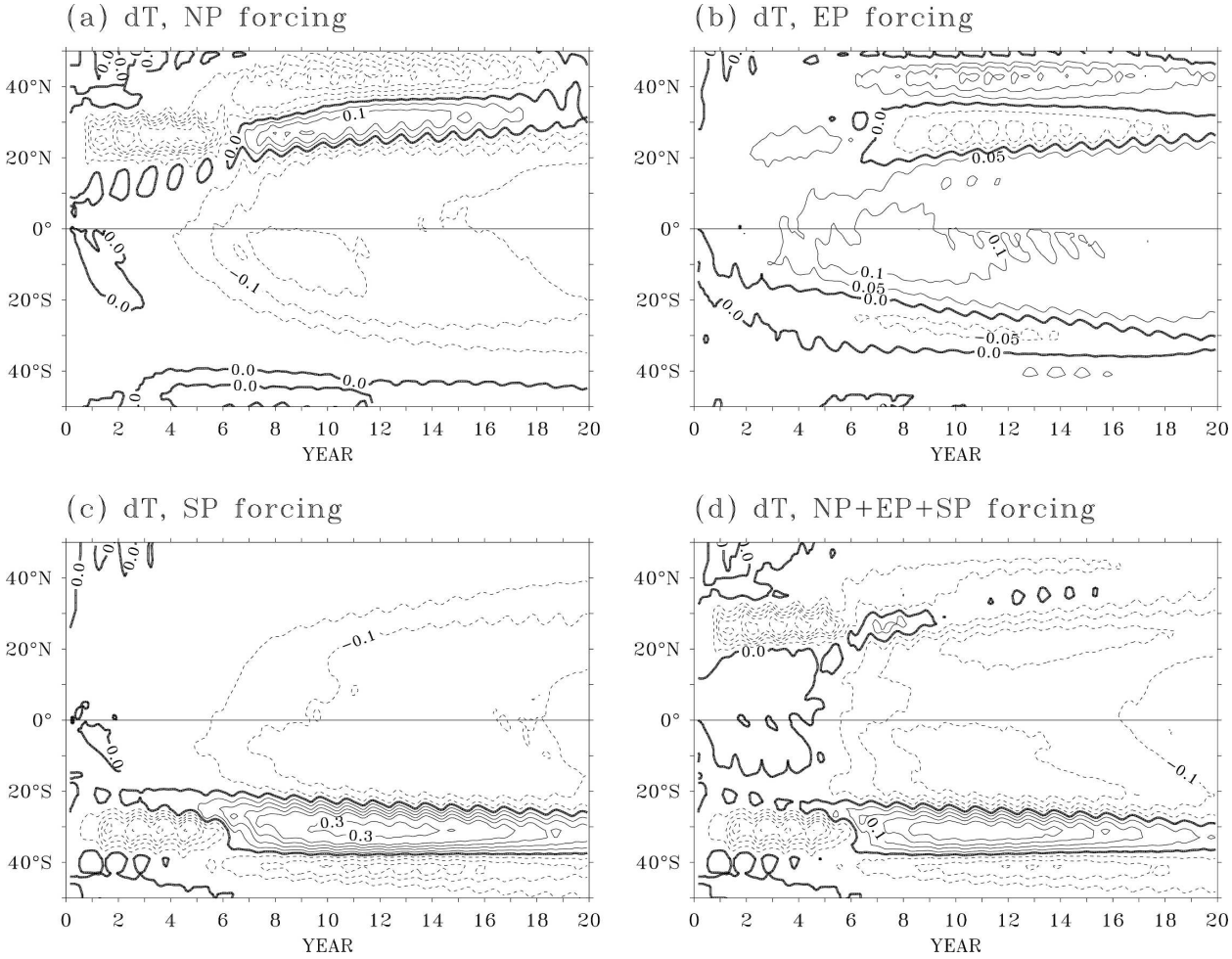

FIG. 13. As in Fig. 12, but for zonal mean temperature anomaly. Contours are 0, ±0.05, ±0.1, ±0.15, and ±0.3°C.

two years) and a slow response (after two years). Model diagnosis showed that both salinity and temperature anomalies are driven by anomalous vertical mixing during the fast response but by anomalous salt and heat advection during the slow response.

As shown in Fig. 1a, the EmP anomalies extended in a wide range of the tropical and subtropical Pacific. Are the EmP anomalies in our experiments sensitive to their locations in the Pacific? To answer this question, additional experiments were conducted. When forced by negative EmP anomalies in the central equatorial Pacific, the structures and evolution of salinity and temperature anomalies were very similar to those forced by the negative EmP anomaly in the western equatorial Pacific. When the positive EmP anomaly in region NP in the North Pacific was shifted 10° northward, the salinity and temperature responses did not change much either. The differences are that the salinity and temperature anomalies can penetrate deeper in the subtropical North Pacific due to steeper thermocline slope at higher latitudes; the cooling propagating via Kelvin waves along the western boundary and the equator is located in a deeper thermocline; the propagation speed is faster due to the contribution of the Equatorial Undercurrent. When the positive EmP anomaly in region SP in the western South Pacific was shifted to the eastern South Pacific near 20°S–110°W, the warming and cooling due to spindown of the subtropical gyre and the cooling starting in the eastern equatorial Pacific appear to be similar to those in the experiment forced with anomalous EmP in region SP. The differences are that the warming in the subtropical South Pacific can easily penetrate into the central equatorial Pacific so that the propagation of cold anomalies from the eastern equatorial Pacific is blocked.

It should be noted, however, that the response of the Pacific to anomalous EmP discussed in this section is based on experiments conducted with flux boundary conditions at the surface. In nature, the temperature response of the Pacific to anomalous EmP may be

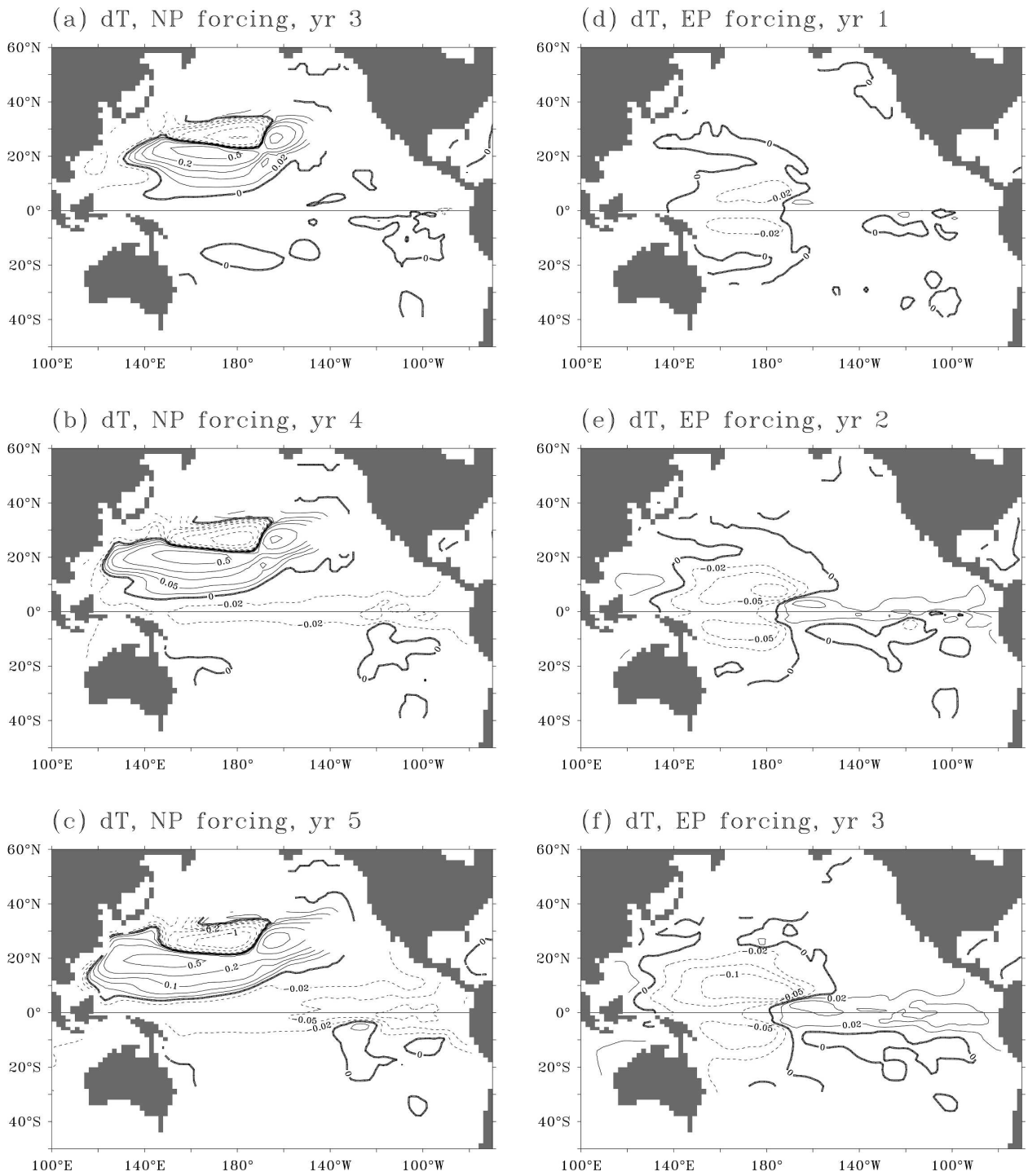

FIG. 14. Temperature anomaly on the 26-σ_θ isopycnal at (a) year 3, (b) year 4, and (c) year 5 in expt NP and at (d) year 1, (e) year 2, and (f) year 3 in expt EP. Contours are 0, ±0.02, ±0.05, ±0.1, ±0.2, ±0.5°C.

damped by changes in surface heat flux or amplified by a feedback from atmospheric freshwater flux since the ocean and atmosphere are a coupled system. To estimate whether the oceanic response to anomalous EmP is sensitive to heat flux damping from the atmosphere, we repeated the experiment ALL with SSTs restored to the observed climatology (experiment RST, Table 1). Results show that SST anomalies were reduced in mag-

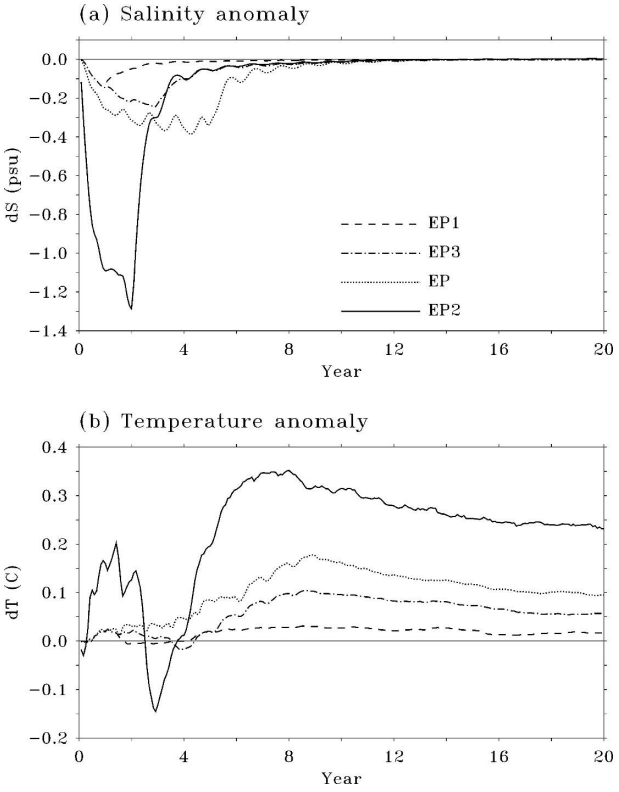

FIG. 15. (a) Salinity anomalies (psu) in the equatorial Pacific (region EP) in expts EP1, EP3, EP5, and EP2. (b) As in (a), but for temperature anomalies (°C).

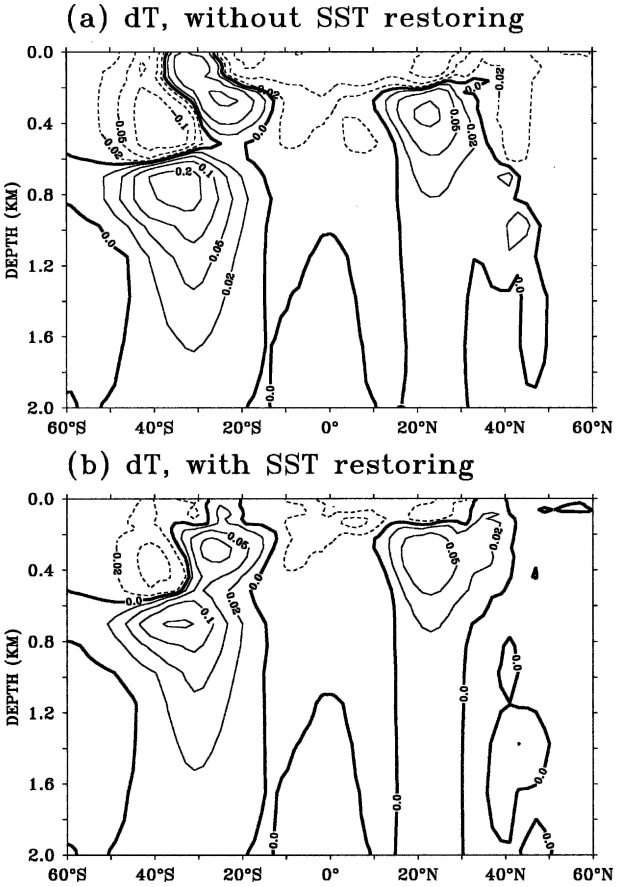

FIG. 16. (a) Zonal average (1–20 yr) temperature anomaly in expt ALL. (b) As in (a), but for experiment RST. Contours are 0, ±0.02, ±0.05, ±0.1, and ±0.2°C.

nitude due to the SST restoring boundary condition, but their spatial structure and evolution were very similar to those in experiment ALL. For example, the 0.3° and 0.5°C cooling in the western North and South Pacific in experiment ALL (Fig. 8d) was reduced to 0.1° and 0.2°C (not shown), respectively, in experiment RST; the 0.2° and 0.6°C warming in the eastern North and South Pacific, respectively, in ALL was reduced to 0.1°C in RST; and the 0.1°C cooling of in the tropical Pacific in ALL was reduced to 0.05°C in RST. The salinity and temperature anomalies in the thermocline, however, were not affected much by the SST restoring. The salinity anomalies in RST (not shown) were almost the same as those in ALL. The temperature anomalies in the thermocline in RST (Fig. 16a) were also similar to those in ALL (Fig. 16b) and their spatial structures were similar to those in ALL. The temperature anomalies, however, became slightly smaller and penetrated less in the upper ocean. This comparison shows that SST anomalies forced by anomalous EmP may be damped by atmospheric heat fluxing damping, but the temperature anomalies can penetrate into the thermocline and persist for many years.

Last, the model resolution in the equatorial and western boundary regions in our experiments is relatively coarse so that coastal and equatorial Kelvin waves and western boundary currents may not have been resolved fully. This may affect the magnitude and time scale of the temperature anomalies in our experiments.

8. Summary

The responses of the upper Pacific Ocean to idealized net atmospheric freshwater (evaporation minus precipitation minus river runoff) were studied in a series of eight experiments, each 20 years long, with the MIT OGCM. The locations and strengths of idealized EmP anomalies were based on observed estimates of EmP since 1988.

Salinity and temperature responded differently to the EmP forcings in our experiments. The response of the Pacific Ocean was to change local salinity initially via

vertical mixing, and then to change remote salinity via salt advection due to mean ocean circulation. The redistribution of anomalous EmP (and therefore salinity) resulted in basinwide anomalous ocean currents, which finally resulted in anomalous temperature locally and remotely.

When evaporation increased or precipitation decreased in the subtropical North and South Pacific, surface salinity increased in the subtropical North and South Pacific. As salinity increased, density also increased in the subtropical North and South Pacific and, therefore, the subtropical gyres spun down. As a result, SST increased in the eastern North and South Pacific, while it decreased in the western North and South Pacific. The cold temperature anomalies generated in the subtropical North and South Pacific subducted and propagated to the tropical Pacific via coastal Kelvin waves along the western boundaries and via equatorial Kelvin waves in the equatorial thermocline. After equatorial Kelvin waves reached the eastern boundary, temperature decreased in the eastern equatorial Pacific. Then, the cold temperature anomalies upwelled to the surface, and traveled westward along the SEC and by Rossby waves while stretching toward the subtropical North and South Pacific.

When precipitation increased or evaporation decreased in the tropical Pacific, surface salinity decreased in both the tropical and subtropical Pacific. The maximum decrease, however, was located near 10°N and 10°S since divergent Ekman flows advected salinity anomalies from the equator toward the subtropics. In contrast, SST increased in the tropical Pacific between 20°S and 20°N and in the western North (30°–50°N) and South (40°–30°S) Pacific; it decreased in the eastern North Pacific near 30°N and the subtropical South Pacific near 30°S. The warming in the tropical Pacific was largely due to a weakened SEC. The warming and cooling in the subtropical North and South Pacific were associated with the spinup of subtropical gyre circulations. Salinity and temperature anomalies generated in the tropical Pacific were advected to the subtropical North and South Pacific by the divergent Ekman flows, the Kuroshio, and the Eastern Australia Current.

The correlation between SSS and SST anomalies in our OGCM experiments was generally negative in the region where EmP anomaly was applied (Figs. 3 and 15). This is consistent with the conclusions in Yang et al. (1999) and Huang and Mehta (2004, 2005). In nature, the correlation would be determined not only by local anomalous EmP forcing, but also by remote anomalous EmP forcing because of the slow response of ocean circulations.

The salinity and temperature responses to anomalous EmP were linear with respect to the magnitude and duration of applied EmP anomalies in our experiments: Salinity and temperature anomalies forced jointly by anomalous EmP at different locations were approximately equal to the sum of these anomalies forced by anomalous EmP at each individual location. The magnitude of salinity and temperature anomalies was also proportional to the total EmP input to the ocean.

In our experiments, the oceanic response in the thermocline did not appear to be sensitive to the flux or restoring SST boundary condition, although the model SST response was weakened when a restoring SST boundary condition was applied.

The results described and discussed in this paper appear to verify our hypothesis that anomalous EmP may cause a remote response in salinity and temperature due to anomalous salt and heat advection, and due to Kelvin and Rossby waves. More important, the temperature response to anomalous EmP was much slower than the salinity response as shown in Fig. 15 because of a slow adjustment of ocean currents. The response of the Pacific Ocean to remote anomalous EmP may take one or more decades, which strongly suggests that anomalous EmP and salinity can play an important role in climate variability at decadal and longer time scales. These results were consistent with the Huang and Mehta (2004) finding that the Indo–Pacific warm pool temperature responded at a slow time scale to imposed EmP forcing. Since the atmosphere is very sensitive to SST changes in the tropical Pacific, especially in the Indo–Pacific warm pool, the anomalous EmP may play an important role in ocean and climate variability at the decadal time scale. However, the role of EmP in the observed, decadal variance of SST remains to be carefully assessed.

Acknowledgments. The authors thank Z. Liu for his comments and suggestions, which helped us in improving our experiment design and model diagnoses. The authors also thank two anonymous reviewers for their valuable and thought-provoking comments. Authors BH and VM were supported by NASA Grants NAG5-11785 and NAG5-12729, and NS was supported by National Science Foundation Grant OCE00-82543, U.S. Department of Energy Office of Science (BER) Grants DE-FG03-01ER63255 and DE-FG02-04ER63862, and National Oceanic and Atmospheric Administration Grant NA17RJ1231. The views expressed herein are those of the authors and do not necessarily reflect the views of NSF, DOE, or NOAA, or any of their subagencies.

APPENDIX

Notation

ALL	experiment with combined anomalous EmP in NP, EP, and SP
CTR	control
EAC	Eastern Australia Current
EmP	evaporation minus evaporation minus river runoff
EP, EP1, EP2, EP3	experiments with anomalous EmP in equatorial Pacific region (Table 1)
ENSO	El Niño–Southern Oscillation
KPP	*K*-profile parameterization
NP	experiment with anomalous EmP in North Pacific region
OGCM	ocean general circulation model
PTB	perturbation
RST	experiment with restoring SST boundary condition
SEC	South Equatorial Current
SP	experiment with anomalous EmP in South Pacific region
SSS	sea surface salinity
SST	sea surface temperature

REFERENCES

Atlas, R., R. N. Hoffman, S. C. Bloom, J. C. Jusem, and J. Ardizzone, 1996: A multiyear global surface wind velocity dataset using SSM/I wind observations. *Bull. Amer. Meteor. Soc.,* **77,** 869–882.

Cessi, P., and S. Louazel, 2001: Decadal oceanic response to stochastic wind forcing. *J. Phys. Oceanogr.,* **31,** 3020–3029.

Chou, S.-H., C.-L. Shie, R. M. Atlas, and J. Ardizzone, 1997: Air–sea fluxes retrieved from special sensor microwave imager data. *J. Geophys. Res.,* **102,** 12 705–12 726.

Dai, A., and K. E. Trenberth, 2002: Estimates of freshwater discharge from continents: Latitudinal and seasonal variations. *J. Hydrometeor.,* **3,** 660–687.

da Silva, A. M., C. C. Young, and S. Levitus, 1994: *Atlas of Surface Maine Data 1994*. NOAA Atlas NESDIS 6-8, 912 pp.

Deser, C., M. A. Alexander, and M. S. Timlin, 1996: Upper-ocean thermal variations in the North Pacific during 1970-1991. *J. Climate,* **9,** 1840–1855.

Frankignoul, C., P. Muller, and E. Zorita, 1997: A simple model of the decadal response of the ocean to stochastic wind forcing. *J. Phys. Oceanogr.,* **27,** 1533–1546.

Goldsbrough, G. R., 1933: Ocean currents produced by evaporation and precipitation. *Proc. Roy. Soc. London,* **A141,** 512–517.

Gu, D., and S. G. H. Philander, 1997: Interdecadal climate fluctuations that depend on exchange between the Tropics and extratropics. *Science,* **275,** 805–807.

Hall, A., and S. Manabe, 1997: Can local linear stochastic theory explain sea surface temperature and salinity variability? *Climate Dyn.,* **13,** 167–180.

Hazeleger, W., M. Visbeck, M. Cane, A. Karspeck, and N. Naik, 2001: Decadal upper ocean temperature variability in the tropical Pacific. *J. Geophys. Res.,* **106,** 8971–8988.

Hellerman, S., and M. Rosenstein, 1983: Normal monthly wind stress over the World Ocean with error estimates. *J. Phys. Oceanogr.,* **13,** 1093–1104.

Huang, B., and Z. Liu 1999: Pacific subtropical–tropical water exchange in the National Centers for Environmental Prediction ocean model. *J. Geophys. Res.*, **104** (C5), 11 065–11 076.

——, and V. M. Mehta, 2004: The response of the Indo-Pacific warm pool to interannual variations in net atmospheric freshwater. *J. Geophys. Res.,* **109,** C06022, doi:10.1029/2003JC002114.

——, and ——, 2005: Response of the Pacific and Atlantic Oceans to interannual variations in net atmospheric freshwater. *J. Geophys. Res.,* **110,** C08008, doi:10.1029/2004JC002830.

——, P. H. Stone, S. P. Sokolov, and I. V. Kamenkovich, 2003: The ocean heat uptake in transient climate change: Mechanisms and uncertainty due to subgrid-scale eddy mixing. *J. Climate,* **16,** 3344–3356.

Huang, R. X., 1993: Real freshwater flux as a natural boundary condition for the salinity balance and thermohaline circulation forced by evaporation and precipitation. *J. Phys. Oceanogr.,* **23,** 2428–2446.

Huffman, G. J., and Coauthors, 1997: The Global Precipitation Climatology Project (GPCP) Combined Precipitation Data Set. *Bull. Amer. Meteor. Soc.,* **78,** 5–20.

Jiang, S., P. H. Stone, and P. Malannotte-Rizzoli, 1999: An assessment of the Geophysical Fluid Dynamics Laboratory ocean model with coarse resolution: Annual-mean climatology. *J. Geophys. Res.,* **104,** 25 623–25 645.

Jin, F.-F., 1997: A theory of interdecadal climate variability of the North Pacific ocean–atmosphere system. *J. Climate,* **10,** 1821–1835.

——, S.-I. An, A. Timmermann, and J. Zhao, 2003: Strong El Niño events and non-linear dynamical heating. *Geophys. Res. Lett.,* **30,** 1120, doi:10.1029/2002GL016356.

Junge, M. M., J.-S. von Storch, and J. M. Oberhumber, 2000: Large-scale variability of the main thermocline excited by stochastic wind stress forcing. *J. Climate,* **13,** 2833–2840.

Kleeman, R., J. P. McCreary, and B. A. Klinger, 1999: A mechanism for generating ENSO decadal variability. *Geophys. Res. Lett.,* **26,** 1743–1746.

Large, W. G., J. C. McWilliams, and S. C. Doney, 1999: Oceanic vertical mixing: A review and a model with non-local boundary layer parameterization. *Rev. Geophys.,* **32,** 363–403.

Latif, M., and T. P. Barnett, 1994: Causes of decadal climate variability over the North Pacific and North America. *Science,* **266,** 634–637.

——, and ——, 1996: Decadal climate variability over the North Pacific and North America: Dynamics and predictability. *J. Climate,* **9,** 2407–2423.

Levitus, S., and T. Boyer, 1994: *Temperature*. Vol. 4, *World Ocean Atlas 1994,* NOAA Atlas NESDIS 4, 117 pp.

——, R. Burgett, and T. Boyer, 1994: *Salinity*. Vol. 3, *World Ocean Atlas 1994,* NOAA Atlas NESDIS 3, 99 pp.

Lindstrom, E., R. Lukas, R. Fine, E. Firing, S. Godfrey, G. Meyers, and M. Tsuchiya, 1987: The western equatorial Pacific Ocean circulation study. *Nature,* **330,** 533–537.

Liu, Z., 1994: A simple model of mass exchange between the

subtropical and tropical ocean. *J. Phys. Oceanogr.,* **24,** 1153–1165.

Lu, P., and J. P. McCreary, 1995: Influence of the ITCZ on the flow of thermocline water from the subtropical to the equatorial Pacific Ocean. *J. Phys. Oceanogr.,* **25,** 3076–3088.

Lukas, R., and E. Lindstrom, 1991: The mixed layer of the western equatorial Pacific Ocean. *J. Geophys. Res.,* **96,** 3343–3357.

Marshall, J., A. Adcroft, C. Hill, L. Perelman, and C. Heisey, 1997: A finite volume, incompressible Navier Stokes model for studies of the ocean on parallel computers. *J. Geophys. Res.,* **102,** 5753–5766.

Schneider, N., 2000: A decadal spiciness mode in the Tropics. *Geophys. Res. Lett.,* **27,** 257–260.

——, 2004: The response of tropical climate to the equatorial emergence of spiciness anomalies. *J. Climate,* **17,** 1083–1095.

——, and T. Barnett, 1995: The competition of freshwater and radiation in forcing the ocean during El Niño. *J. Climate,* **8,** 980–992.

——, A. J. Miller, M. A. Alexander, and C. Deser, 1999: Subduction of decadal North Pacific temperature anomalies: Observations and dynamics. *J. Phys. Oceanogr.,* **29,** 1056–1070.

Stommel, H. M., 1984: The delicate interplay between wind-stress and buoyancy input in ocean circulation: The Goldsbrough variation. *Tellus,* **46A,** 111–119.

Timmermann, A., F.-F. Jin, and J. Abshagen, 2003: A nonlinear theory for El Niño bursting. *J. Atmos. Sci.,* **60,** 152–165.

Wu, L., Z. Liu, R. Gallimore, R. Jacob, D. Lee, and Y. Zhong, 2003: Pacific decadal variability: The tropical Pacific mode and the North Pacific mode. *J. Climate,* **16,** 1101–1120.

Yang, S., K.-M. Lau, and P. S. Schopf, 1999: Sensitivity of the tropical Pacific Ocean to precipitation-induced freshwater flux. *Climate Dyn.,* **15,** 737–750.

Yeager, S. G., and W. G. Large, 2004: Later-winter generation of spiciness on subducted isopycnals. *J. Phys. Oceanogr.,* **34,** 1528–1547.

Zhang, R. H., L. M. Rothstein, and A. J. Busalacchi, 1999: Interannual and decadal variability of the subsurface thermal structure in the Pacific Ocean: 1961–90. *Climate Dyn.,* **15,** 703–717.